International Journal of Mass Spectrometry 330–332 (2012) 6–15

Contents lists available at SciVerse ScienceDirect

International Journal of Mass Spectrometry

journal homepage: www.elsevier.com/locate/ijms

Infrared multiple photon dissociation spectroscopy of protonated histidine and 4-phenyl imidazole

Murat Citir[a,b], Christopher S. Hinton[a], Jos Oomens[c,d], Jeffrey D. Steill[c], P.B. Armentrout[a,*]

[a] Department of Chemistry, University of Utah, Salt Lake City, UT 84112, United States
[b] Abdullah Gül University, Melikgazi/Kayseri, 38039, Turkey
[c] FOM Institute for Plasma Physics "Rijnhuizen", Edisonbaan 14, 3439 MN Nieuwegein, The Netherlands
[d] Van't Hoff Institute for Molecular Sciences, University of Amsterdam, Amsterdam, The Netherlands

ARTICLE INFO

Article history:
Received 27 April 2012
Received in revised form 31 May 2012
Accepted 5 June 2012
Available online 23 June 2012

Keywords:
Histamine
Histidine
Imidazole
IRMPD

ABSTRACT

The gas-phase structures of protonated histidine (His) and the side-chain model, protonated 4-phenyl imidazole (PhIm), are examined by infrared multiple photon dissociation (IRMPD) action spectroscopy utilizing light generated by the free electron laser FELIX. To identify the structures present in the experimental studies, the measured IRMPD spectra are compared to spectra calculated at a B3LYP/6–311+G(d,p) level of theory. Relative energies of various conformers are provided by single point energy calculations carried out at the B3LYP, B3P86, and MP2(full) levels using the 6–311+G(2d,2p) basis set. On the basis of these experiments and calculations, the IRMPD action spectrum for H^+(His) is characterized by a mixture of [N_π,N_α] and [N_π,CO] conformers, with the former dominating. These conformers have the protonated nitrogen atom of imidazole adjacent to the side-chain (N_π) hydrogen bonding to the backbone amino nitrogen (N_α) and to the backbone carbonyl oxygen, respectively. Comparison of the present results to recent IRMPD studies of protonated histamine, the radical $His^{\bullet+}$ cation, H^+(HisArg), H_2^{2+}(HisArg), and M^+(His), where $M^+ = Li^+$, Na^+, K^+, Rb^+, and Cs^+, allows evaluation of the vibrational motions associated with the observed bands.

1. Introduction

Histidine (His) is chemically one of the most flexible protein residues because the imidazole side chain can function as both an acid and base near neutral pH [1]. The histidine molecule presents three potential coordination sites in aqueous solution. The carboxyl group ($pK_a = 1.9$), the imidazole nitrogen ($pK_a = 6.1$), and the amino nitrogen ($pK_a = 9.1$) become available for complexation as pH increases. The acid–base properties of a biomolecule affect physicochemical activities such as solubility, hydrophobicity, and electrostatic interactions that directly impact the biological activity of the molecule in a living system. Because the pK_a of the imidazolium form is around 6, histidine can undergo protonation and deprotonation reactions at physiological pH. Therefore, it functions as a competent proton-transfer mediator in various proteins [2–5]. Histidine also serves as both a hydrogen-bond donor and an acceptor, and this hydrogen-bonding property is of importance in proton-transfer reactions [5] and in organizing the active centers of enzymes. As a consequence, histidine is often found at the catalytic sites of protein enzymes.

In recent years, the structures of many proteins have been studied by X-ray crystallography; however, because of the poor sensitivity of X-ray crystallography in detecting hydrogen atoms, the protonation structures and hydrogen-bonding interactions of amino acid side chains are not well resolved in many cases. To obtain such information, vibrational spectroscopy is a powerful method as it is more sensitive to chemical bonds and molecular interactions. In the case of histidine, its protonation state, metal binding, and hydrogen bonding interactions have been investigated using both Raman [6–18] and Fourier transform infrared (FTIR) [19] spectroscopy. Huang et al. [20] investigated the neutral, protonated, and deprotonated histidine conformers in the gas phase using time-dependent density functional theory (TDDFT) to calculate the electronic spectra and charge-transfer processes. Also, Hasegawa et al. [21] studied 4-methylimidazole (a simple model compound of the histidine side chain) and its different protonation forms using FTIR and Raman spectra for systematic investigation of vibrational markers of the protonation state of histidine.

Infrared multiple photon dissociation (IRMPD) spectroscopy has been used to probe the structures of ionized complexes in the gas phase and can be a powerful tool for understanding ion–protein interactions. An important advantage of this technique is the ability to investigate the structures of biomolecules in isolation, where complicating structural effects of solvent and counter-ions

* Corresponding author. Tel.: +1 801 581 7885; fax: +1 801 581 8433.
E-mail address: armentrout@chem.utah.edu (P.B. Armentrout).

1387-3806/$ – see front matter © 2012 Elsevier B.V. All rights reserved.
http://dx.doi.org/10.1016/j.ijms.2012.06.002

are absent. Recently, gas-phase structures of protonated histamine [22], histidine radical cation ($His^{\bullet+}$) [23], H^+(HisArg) and H_2^{2+}(HisArg) [24], and M^+(His) [25], where $M^+ = Li^+$, Na^+, K^+, Rb^+, and Cs^+, have all been investigated by IRMPD spectroscopy utilizing light generated by a free electron laser. In the present study, we measure the IRMPD action spectra for photodissociation of protonated His and 4-phenyl imidazole (PhIm), where the latter provides a model for assessing the vibrations of the imidazole side-chain ring. Conformations of these molecules are identified by comparing the experimental spectra to IR spectra of the low-lying structures of the cationized His and PhIm complexes predicted by quantum chemical calculations at the B3LYP/6–311+G(d,p) level of theory. IRMPD action spectra for H^+(His) and H^+(PhIm) are also compared to the previous results for H^+(histamine), $His^{\bullet+}$, H^+(HisArg), H_2^{2+}(HisArg), and M^+(His), where $M^+ = Li^+$, Na^+, K^+, Rb^+, and Cs^+.

2. Experimental and computational

2.1. Mass spectrometry and photodissociation

Experiments were performed using the Free Electron Laser for Infrared eXperiments (FELIX) [26] in combination with a home-built Fourier transform ion cyclotron resonance (FTICR) mass spectrometer, which has been described in detail elsewhere [27–29]. Protonated histidine and protonated phenyl imidazole complexes were generated using a Z-spray (Micromass UK Ltd.) electrospray ionization source. Solutions used were 1.0–3.0 mM His with 1 mM acetic acid in 50% MeOH and 50% H_2O for H^+(His) and 1.0 mM phenyl imidazole acidified with acetic acid in 58% MeOH and 42% H_2O for H^+(PhIm). Solution flow rates were about 10 μL/min and the electrospray needle was held at a voltage of ~3.2 kV. Ions were accumulated in a hexapole trap for about 4 s followed by pulsed extraction through a quadrupole bender prior to being injected into the ICR cell via a radio frequency (rf) octopole ion guide. Electrostatic pulsing of the dc bias of the ion transfer octopole allows ions to be captured in the ICR cell without the use of a gas pulse [28]. In contrast to the conventional gas pulsing method to stop the ions, this technique does not cause collisional heating of the ions. The precursor ions were mass selected using stored waveform inverse Fourier transform (SWIFT) techniques and irradiated by the FEL at pulse energies of 50 mJ per macropulse of 5 μs duration, although they fell off to about 20 mJ toward the blue edge of the scan range. Complexes were irradiated for 2–4 s, corresponding to interaction with 10–20 macropulses. The fwhm bandwidth of the laser was typically 0.5% of the central wavelength. For the present experiments, spectra were recorded over the wavelength range 19.4 μm (520 cm^{-1}) to 5.5 μm (1820 cm^{-1}), which can be covered with a single setting of the electron beam energy of FELIX.

2.2. Computational details

Our protocol for finding all low-lying conformations of metal cation–amino acid complexes has been described elsewhere [30]. To find the global energy minimum and all low-energy geometries, a large number of possible conformations were screened using a simulated annealing methodology with the AMBER program and the AMBER force field based on molecular mechanics [31]. All possible structures identified this way were subsequently optimized using NWChem [32] at the HF/3–21G level [33,34]. Unique structures for each system were optimized using Gaussian 09 [35] at the B3LYP/6–31G(d) level of theory [36,37] with the "loose" keyword (maximum step size 0.01 au and an RMS force of 0.0017 au) to facilitate convergence. Unique structures obtained from this procedure were then chosen for higher-level geometry optimization and frequency calculations using DFT at the B3LYP/6–311+G(d,p) level of theory [38]. Single point energy calculations were carried out at the B3LYP, B3P86, and MP2(full) levels using the 6–311+G(2d,2p) basis set [38]. Zero-point vibrational energy (ZPE) corrections were determined using vibrational frequencies calculated at the B3LYP/6–311+G(d,p) level scaled by a factor of 0.989 [39]. Relative energies at 0 K are converted to 298 K free energies using the rigid rotor/harmonic oscillator approximation with rotational constants and vibrational frequencies calculated at the B3LYP/6–311+G(d,p) level. As will be seen below, the relative ΔG_{298} excitation energies are comparable to the analogous differences in the ΔH_0 values.

Vibrational frequencies and intensities were calculated using the harmonic oscillator approximation and analytical derivatives of the energy-minimized Hessian at the B3LYP/6–311+G(d,p) level of theory. Each of the resulting structures was found to have all real harmonic vibrational frequencies at this level of theory indicating that they are local minima on the potential energy surface. For comparison to IRMPD spectra, frequencies were scaled by 0.975 as this scaling factor leads to good agreement between calculated and experimentally well-resolved peaks and is in accord with previous IRMPD studies of amino acid complexes in this spectral region as well [40–45]. Calculated vibrational frequencies are broadened using a 20 cm^{-1} fwhm Gaussian line shape for comparison with experimental spectra.

At the request of a reviewer, we also calculated geometries and single point energies adding a diffuse function for hydrogen, i.e., R/6–311++G(2d,2p)//B3LYP/6–311++G(d,p), where R indicates B3LYP, B3P86, and MP2(full) levels. This is intended to provide a better description of hydrogen bonding, even though previous explorations in our group have indicated that hydrogen diffuse functions have negligible effects on geometries and relative energies [46–49]. In the present case, six conformers of three different types were examined. Structures were essentially unchanged with hydrogen bonds (a total of 16 interactions) changing by −0.0025 to +0.0008 Å, with the average absolute change being 0.0006 ± 0.0007 Å. Relative energies at this level of theory agreed with those presented below within 0.1 kJ/mol in all cases. Furthermore, vibrational frequencies are the same within 0.01%. Because the addition of diffuse functions to the hydrogen atoms introduces little distortions, energy changes, or vibrational shifts, such calculations were not pursued further for any other conformations.

3. Results and discussion

3.1. IRMPD action spectroscopy

The photodissociation spectra of protonated (m/z 156) His both as depletion of the parent ion and the yield for loss of $H_2O + CO$ (m/z 110) (corrected for laser power and uncorrected) are shown in Fig. S1 of the Supporting Information. Very small amounts (>10 times smaller) of just H_2O loss were also detected. These decomposition pathways match the lowest energy products observed in the collision-induced dissociation (CID) spectrum of H^+(His), as observed previously [50,51]. Parent and product ion intensities were monitored as a function of the laser frequency, and the IRMPD yield shown in Fig. S1 and the figures below was calculated as the integrated intensity ratio $I_{110}/(I_{110} + I_{156})$. This was normalized linearly with laser power to roughly account for the change in laser power as a function of photon energy. As shown in Fig. S1, the depletion spectrum of the m/z 156 parent ion is similar to the appearance spectrum of the m/z 110 product ion. The depletion of the parent ion signal exceeds 50% at the most intense resonances. Because the IRMPD yield is normalized for parent ion fluctuations, it exhibits better signal-to-noise ratio than the depletion signal and will be compared to the calculated spectra.

To provide a spectrum characteristic of the imidazole (Im) side-chain of His, we also tried acquiring the IRMPD spectrum of protonated Im. Unfortunately, this molecule is sufficiently small that dissociation is inefficient and no spectrum could be collected. To overcome this size limitation, it would be useful to examine Im substituted at the 4-position to mimic the His side-chain. Simple alkyl-substituted Im are unstable or not readily available, but 4-phenyl imidazole (PhIm) is commercially available. For protonated PhIm, two IR photodissociation pathways were observed corresponding to the loss of HCN (*m*/*z* 118) and 2 HCN (*m*/*z* 91). The sum of these two decomposition pathways is shown as the IRMPD action spectrum below.

3.2. Theoretical results (structures)

The nomenclature used here to identify different structural isomers of H^+(His) is similar to that described previously for the IRMPD study of M^+(His) [25]; however, here the atoms of His are named according to the IUPAC Compendium of Chemical Terminology (Gold Book), in which positions of the nitrogen atoms of the imidazole ring relative to the side chain are denoted by *pros* ('near', abbreviated π and also referred to as N_1) and *tele* ('far', abbreviated τ or N_3) [52], Fig. 1. In addition, conformations of protonated His are identified by their proton binding sites in brackets, followed by a description of the histidine orientation, named by a series of dihedral angles starting from the carboxylic acid hydrogen of the backbone and going to the imidazole side-chain nitrogen (N_π) (∠HOCC, ∠OCCC, ∠CCCC, and ∠CCCN_π, respectively). Dihedral angles are distinguished as cis (c, for angles between 0° and 45°), gauche (g, 45–135°), or trans (t, 135–180°), and + or − indicating their sign when necessary to distinguish similar structures. In some cases, these four dihedral angles are insufficient to distinguish similar conformers and a fifth dihedral angle is added in parentheses to define the electron lone pair orientation of the $N_\alpha H_2$ group. In most conformations, this orientation is cis with respect to the adjacent backbone CC bond, such that only alternate orientations (gauche or trans) are indicated by this fifth dihedral angle.

Eight low-lying and representative higher energy conformations of H^+(His) are illustrated in Fig. 1, with a total of 24 structures shown in Fig. S2 in the Supporting Information. The protonated histidine complex, H^+(His), has a set of low energy structures, [N_π,N_α], in which the protonated imidazole side-chain hydrogen bonds to the backbone amino nitrogen ($N_\pi H\cdots N_\alpha$), Fig. 1. If the proton shifts to N_α, retaining a hydrogen bond to N_π, the [N_α,N_π] conformer is formed. These structures are not shown in Fig. 1 as the only significant distinction from the analogous [N_π,N_α] structures is the position of the bridging proton. Other possible binding motifs are [N_π,CO] and [N_π,OH], in which the protonated imidazole side-chain hydrogen bonds to the backbone carbonyl oxygen ($N_\pi H\cdots OC$) or hydroxyl oxygen ($N_\pi H\cdots OH$). The latter are not shown in Fig. 1 because they resemble the [N_π,CO] structures with the carboxylic group rotated by 180°. Relative Gibbs free energies at 298 K and relative energies at 0 K including zero-point energy (ZPE) corrections with respect to the ground state calculated at three different levels of theory are given in Table 1 for H^+(His). Because the relative Gibbs free energies may be more relevant in describing the experimental distributions, these values are used throughout the discussion below.

At all levels of theory, the ground state (GS) structure for H^+(His) is [N_π,N_α]-tggc, Fig. 1. In addition, there are five other stable geometries having this binding motif. Only slightly higher in energy, 1–5 kJ/mol, is the tgtc conformer. Both the tggc and tgtc structures have similar $N_\pi H\cdots N_\alpha$ hydrogen bond lengths (1.916 and 1.902 Å, respectively), but the former appears to be stabilized by a stronger $N_\alpha H\cdots OC$ interaction, as suggested by bond lengths of 2.272 and 2.420 Å, respectively. [N_π,N_α]-ttgc and tttc conformers are found at slightly higher energies, 4–5 and 5–10 kJ/mol above the GS, respectively, and have slightly longer $N_\pi H\cdots N_\alpha$ hydrogen bond lengths (1.967 and 1.932 Å, respectively). These conformers differ from the lower energy structures by the ∠OCCC dihedral being trans rather than gauche, which rotates the carboxylic acid such that the $N_\alpha H\cdots OC$ hydrogen bond is replaced by a weaker $N_\alpha H\cdots OH$ hydrogen bond, Fig. 1. Finally, the cggc and cgtc conformers have geometries similar to the tggc and tgtc structures, but the hydroxyl hydrogen is rotated such that it no longer interacts with the carbonyl oxygen, Fig. S2, which costs about 31 and 34 kJ/mol, respectively. These conformers have $N_\pi H\cdots N_\alpha$ hydrogen bond lengths of 1.966 and 1.903 Å, respectively. Similar comparisons hold for the six analogous [N_α,N_π] conformers, shown in Fig. S2. At the B3LYP and B3P86 levels, all [N_α,N_π] conformers lie higher in energy than their [N_π,N_α] counterparts, with the [N_α,N_π]-tgtc variant being lowest in energy. In contrast, MP2 calculations find that the [N_α,N_π]-tggc and cgtc conformers are slightly lower in energy than their [N_π,N_α] analogs, with the tggc conformer being lowest of the [N_α,N_π] conformers. The [N_α,N_π] conformers have relatively short $N_\alpha H\cdots N_\pi$ hydrogen bond lengths of 1.63–1.66 Å, indicating that the proton generally prefers to be on the N_π nitrogen.

Eight different [N_π,CO] conformers were located with the ctg_+g_- structure being the lowest at the DFT levels of theory, 2–4 kJ/mol above the GS. This structure has the shortest $N_\pi H\cdots OC$ hydrogen bond length (1.673 Å) among the [N_π,CO] conformers and is stabilized by a $OH\cdots N_\alpha$ hydrogen bond, Fig. 1. The next four conformers in energy are all ttgg with $N_\pi H\cdots OC$ hydrogen bond lengths of 1.78–1.83 Å, Figs. 1 and S2. In these conformers, the hydroxyl group has rotated, losing the $OH\cdots N_\alpha$ hydrogen bond and replacing it with

Table 1
298 K free energies (0 K relative enthalpies) in kJ/mol of low-lying conformers of H^+(His).[a]

Structure	Dihedral	B3LYP	B3P86	MP2(full)
[N_π,N_α]	tggc	**0.0 (0.0)**	**0.0** (*0.4*)	**0.0 (0.0)**
	tgtc	0.6 (0.8)	1.1 (*1.7*)	5.1 (5.3)
	tttc	4.2 (5.5)	4.9 (6.7)	8.7 (10.1)
	ttgc	4.4 (3.9)	5.1 (5.1)	4.1 (3.7)
	cggc	31.0 (30.8)	31.4 (31.6)	29.7 (29.5)
	cgtc	34.8 (35.1)	35.2 (*35.9*)	39.7 (40.0)
TS	tggc	8.2 (6.0)	1.7 **(0.0)**	4.9 (2.8)
([N_π,N_α]	tgtc	7.2 (5.6)	1.5 (0.3)	7.6 (6.0)
→	tttc	15.5 (15.3)	10.1 (10.3)	14.9 (14.7)
[N_α,N_π])	ttgc	17.2 (15.3)	11.4 (9.9)	12.7 (10.8)
	cggc	41.7 (40.0)	35.0 (33.7)	38.2 (36.5)
	cgtc	41.3 (39.6)	35.2 (33.9)	42.3 (40.6)
[N_α,N_π]	tggc	*8.5* (*7.2*)	*5.1* (*4.3*)	2.7 (1.4)
	tgtc	6.6 (*6.0*)	*4.1* (*3.9*)	3.7 (3.1)
	tttc	*17.7* (*18.4*)	*15.8* (*16.9*)	14.1 (*14.8*)
	ttgc	*20.0* (*19.0*)	*17.4* (*16.9*)	*12.8* (*11.9*)
	cggc	*42.4* (*41.4*)	*38.6* (*38.0*)	37.3 (36.3)
	cgtc	40.1 (39.3)	*37.2* (*36.8*)	37.9 (37.0)
[N_π,CO]	ctg_+g_-	3.9 (1.8)	1.7 **(0.0)**	12.9 (10.8)
	ttg_-g_+(g)	4.8 (5.0)	7.3 (7.9)	8.1 (8.3)
	ttg_-g_+(t)	4.9 (4.8)	7.2 (7.4)	11.2 (11.0)
	ttg_+g_-(t)	5.2 (5.9)	6.8 (7.8)	13.9 (14.5)
	ttg_+g_-(g)	8.6 (8.0)	10.5 (10.3)	16.1 (15.4)
	ctg_-g_+	17.7 (15.8)	16.9 (15.4)	23.5 (21.5)
	ctg_-g_+(t)	28.7 (29.6)	30.8 (32.1)	35.1 (36.0)
	cggg	30.0 (30.8)	31.6 (32.8)	34.1 (34.9)
[N_π,OH]	tcg_-g_+(g)	23.1 (26.4)	26.3 (30.0)	23.2 (26.4)
	$tg_-g_+g_-$(t)	29.2 (30.2)	33.1 (34.4)	34.9 (35.8)
	$tg_-g_+g_-$(g)	31.5 (32.3)	35.0 (36.2)	36.7 (37.5)
	$tg_+g_-g_+$(t)	33.5 (35.9)	38.1 (41.0)	36.2 (38.7)

[a] All values calculated at the level of theory indicated using the 6–311+G(2d,2p) basis set with structures and zero-point energies calculated at the B3LYP/6–311+G(d,p) level of theory. Ground state species are identified in bold. Italics indicate species that collapse because the TS energy is lower.

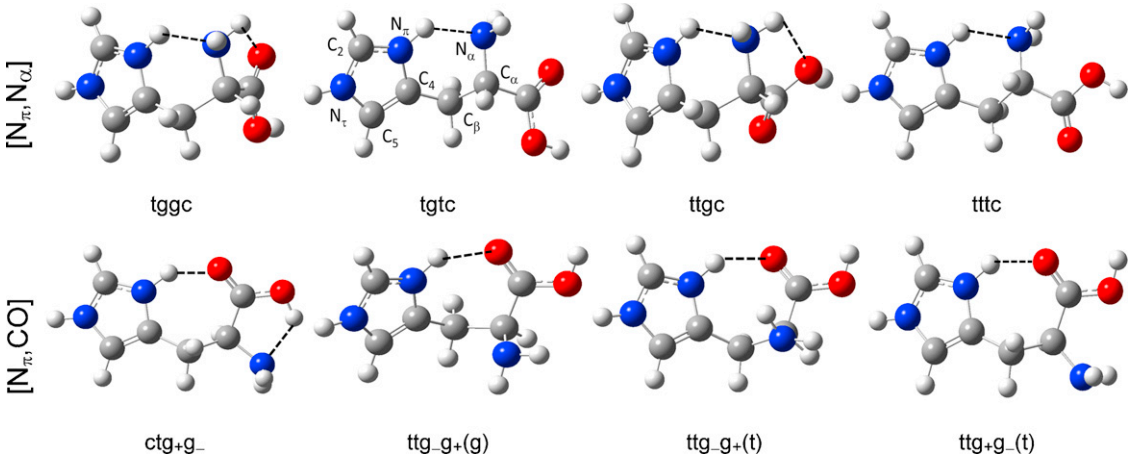

Fig. 1. Structures of the H^+(His) complexes calculated at the B3LYP/6–311+G(d,p) level of theory. Dashed lines indicate hydrogen bonds shorter than 2.3 Å. Atomic labels of protonated histidine are shown in one panel.

an OH···OC interaction augmented by various $N_\alpha H\cdots O(H)$ interactions depending on the orientation of the $N_\alpha H_2$ group, (g) or (t). DFT calculations find that these species lie 5–11 kJ/mol above the GS and 1–9 kJ/mol above the $[N_\pi,CO]$-ctg+g− structure, whereas MP2 calculations find that the lowest energy $[N_\pi,CO]$ conformer is ttg−g+(t) with the ctg+g− variant lying 5 kJ/mol higher. Finally, there are three higher lying conformers, ctg−g+, ctg−g+(t), and cggg, having $N_\pi H\cdots OC$ hydrogen bond lengths of 1.74–1.85 Å, Fig. S2. The lowest of these, ctg−g+, is stabilized by a $OH\cdots N_\alpha$ hydrogen bond such that it lies 10–15 kJ/mol above ctg+g−. The other two lie 21–30 kJ above ctg+g−. Four $[N_\pi,OH]$ conformers have structures similar to the analogous ttgg geometries shown in Fig. 1, with the carboxylic acid group rotated by about 180°. These species lie fairly high in energy, 23–38 kJ/mol above the GS conformer and 15–31 kJ/mol above analogous $[N_\pi,CO]$ conformers, Table 1.

We also carefully examined the proton transfer process that connects the $[N_\pi,N_\alpha]$ and $[N_\alpha,N_\pi]$ conformers, locating the transition state (TS) for all six side-chain orientations, Table 1. B3LYP, B3P86, and MP2(full) level calculations reveal that the barriers ($N_\pi \rightarrow$ TS) are 6–13, 0–6, and 2–9 kJ/mol, respectively. At the B3LYP level, except for tgtc and cgtc, the 298 K free energies of these TSs lie *below* that for the associated $[N_\alpha,N_\pi]$ conformer, indicating that the latter collapse with no energy barrier to the analogous $[N_\pi,N_\alpha]$ form. At the B3P86 level, all six $[N_\alpha,N_\pi]$ conformers collapse to the $[N_\pi,N_\alpha]$ forms, whereas MP2(full) theory suggests that only the $[N_\alpha,N_\pi]$-ttgc conformer will collapse. Similar trends are found for the 0 K enthalpies.

Fig. 2 shows the potential energy surfaces along the N_π–H–N_α coordinate linking all six $[N_\pi,N_\alpha]$ and $[N_\alpha,N_\pi]$ conformers calculated at the B3LYP/6–311+G(d,p) level by explicitly controlling the N_π—H bond distance and allowing all other degrees of freedom to optimize. For comparison, the potential for protonated histamine, which is His without the carboxylic acid on the α-carbon, is also included. It can be seen that in all cases two separate minima in an asymmetric double-well potential exist. Therefore the relative stabilities and instabilities noted above are the result of differences in zero point energies. This is partially indicated by the zero of the scale in Fig. 2, which is set to the zero point energy of the harmonically calculated proton motion of the $[N_\pi,N_\alpha]$ conformers (scaled frequencies ranging from 3025 to 3170 cm^{-1}). Anharmonic frequency calculations for the $[N_\pi,N_\alpha]$-tggc conformer find a modest shift from 3085 cm^{-1} (harmonic, 0.975 scaling) to 2937 cm^{-1} (anharmonic, unscaled). Despite this, use of harmonic frequencies on such an anharmonic potential is not exact and use of the harmonic frequency for proton motion of the $[N_\alpha,N_\pi]$ conformers would place the zero differently for each conformer. These frequencies range from 2338 to 2465 cm^{-1} (scaled), which places the zero point level for these conformers roughly 14 kJ/mol above the bottom of the $[N_\alpha,N_\pi]$ potential wells.

3.3. Comparison of experimental and theoretical IR spectra: H^+(His)

The power-corrected experimental spectrum for H^+(His) is shown in Fig. 3 and exhibits major peaks at 1778, 1609, 1399, 1306, 1132, 822, 676, and 609 cm^{-1}. Additional weaker bands are observed at 1747, 1433, 1340, ~990, ~923, and ~742 cm^{-1}, with an unresolved shoulder at 1079 cm^{-1}. Fig. 3 compares the experimental spectrum with those calculated for the most stable conformers of $[N_\pi,N_\alpha]$, $[N_\alpha,N_\pi]$, and $[N_\pi,CO]$, which are the most likely conformers to be populated along with $[N_\pi,N_\alpha]$-tgtc (and possibly ttgc) on the basis of the theoretical 298 K free energies, Table 1. Fig. S3 shows the predicted spectra of all conformations for comparison, and Table 2 makes qualitative assignments of bands predicted for the $[N_\pi,N_\alpha]$-tggc and $[N_\pi,CO]$-ctg+g− conformers on the basis of visualizing the molecular motions. Fig. S3 shows that the four lowest structures for $[N_\pi,N_\alpha]$, all txxc where *x* = g or t, have

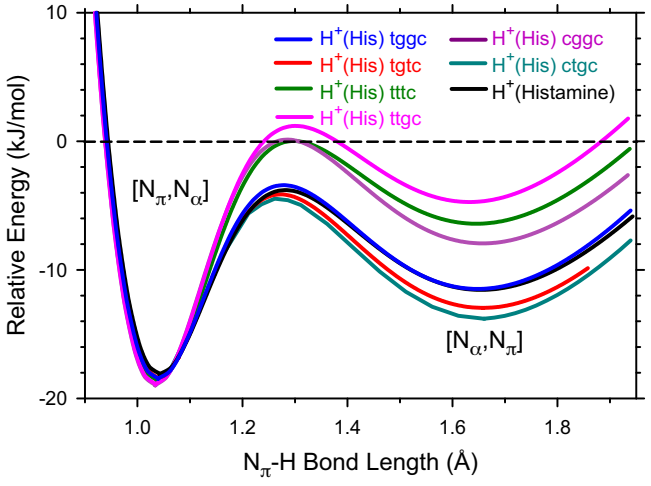

Fig. 2. Relaxed potential energy surfaces of H^+(His) and H^+(histamine) along the N_π–H–N_α coordinate linking the $[N_\pi,N_\alpha]$ (left side) and $[N_\alpha,N_\pi]$ (right side) conformers calculated at the B3LYP/6–311+G(d,p) level. The energy zero is set to the zero point energy of the harmonic frequency in the $[N_\pi,N_\alpha]$ potential well.

Table 2
Experimental vibrational frequencies (cm^{-1}) of H^+(His) compared to B3LYP/6–311+G(d,p) frequencies of the [N_π,N_α]-tggc and [N_π,CO]-ctg$_+$g$_-$ conformers.

H^+(His) ν_{exp} [a]	H^+(His), ν_{cal} [b] [N_π,N_α]-tggc	H^+(His), ν_{cal} [b] [N_π,CO]-ctg$_+$g$_-$	Vibration[c]
1778	1775 (266)	–	σ_{CO}
1747	–	1736 (291)	σ_{CO}/β_{NH} (N_π)
1609	1610 (76)	1608 (129)	σ_{CC} (C_4C_5)/β_{NH} (N_π,N_τ)/β_{CH} (C_5) = ν_5(Im)
	1593 (79)	1623 (44)	β_{NH_2} (scissor)
	1512 (12)	1516 (8)	σ_{CN} (C_2)/β_{CH} (C_2,C_5) = ν_6(Im)
1433	1461 (15)	1459 (14)	β_{NH} (N_τ)/σ_{CN} (N_τ)
	1444 (18)	1446 (16)	β_{CH_2} (scissor, C_β)
	–	1408 (19)	β_{NH} (N_π)/σ_{CN} (C_4N_π)/β_{COH}
1399	1392 (54)	–	β_{NH} (N_π)/σ_{CN} (N_π) = ν_7(Im)
	1391 (26)	–	β_{CH} (C_α)/β_{CH_2} (wag)/τ_{NH2}
	–	1387 (568)	β_{COH}
	–	1367 (7)	β_{CH} (C_α)/β_{NH2} (twist)
1340	1341 (1)	1329 (3)	β_{CH_2} (wag)/β_{CH} (C_α)
1306	1299 (31)	1309, 1267 (7.48)	β_{CH} (C_α)/β_{CH} (C_β)/β(Im)
	1292 (21)	1217 (2)	β_{COH}/β_{CH} (C_α)
	1252 (4)	–	σ_{CCN} (C_4)/β_{CH} (C_α)/β_{NH_2} (twist)/β_{CH2} (twist)
	1239 (6)	1249 (20)	σ_{CN} (C_5N_τ)/β_{CH} (C_5)/β_{CH2} (wag) = ν_{10}(Im)
	1205 (2)	1185 (3)	β_{CH_2} (twist)/β_{CH} (C_α) = ν_8(Im)
	1188 (17)	1150 (2)	β_{NH_2} (twist)/β_{CH} (C_α)/β_{CH} (C_β)
	1164 (8)	1165 (4)	β_{CH} (C_2)/β_{NH} (N_τ) = ν_9(Im)
1132	1139 (175)	–	$\beta_{COH}/\sigma_{CO(H)}$
	1107 (130)	1126 (172)	β_{NH} (N_π)/β_{NH} (N_τ)/σ_{CN} (C_2)/β_{CH} (C_5) = ν_{12}(Im)
1079	–	1079 (20)	σ_{CN} (N_α)
	–	1067 (17)	σ_{CN} (C_5N_τ)/β_{CH} (C_5)/β_{NH} (N_τ)
	1066 (4)	–	σ_{CN} (C_5N_τ)/β_{CH} (C_5) and σ_{CN} (N_α) = ν_{11}(Im)
	1061 (40)	–	σ_{CN} (C_5N_τ)/β_{CH} (C_5) and σ_{CN} (N_α) = ν_{11}(Im)
990	–	1009 (38)	σ_{CC} ($C_\alpha C_\beta$)/β_{NH_2} (twist)
	1002 (107)	–	σ_{CN} (N_π,sym)/γ_{NH} (N_π)/β_{NH_2} (wag) = ν_{14}(Im)
	–	987 (30)	γ_{NH} (N_π) = ν_{21}(Im)
	973 (55)	–	β_{NH_2} (wag)/σ_{CN} (CN_α)
923	955 (53)	960 (80)	γ_{NH} (N_π)/β_{CH} (C_2) = ν_{21}(Im)
	946 (41)	933 (18)	$\tau_{NH_2}/\beta_{CH_2}/\gamma_{NH}$ (N_π)
	925 (14)	924 (9)	β ($CN_\tau C$) = ν_{15}(Im)
	889 (3)	–	σ_{CC} ($C_\beta C_\alpha$)
	–	882 (83)	γ_{COH}
	829 (6)	–	β_{CC} (C_β)/β_{CH} (C_2,twist)/β_{NH2} (wag)
822	823 (39)	830 (33)	γ_{CH} (in phase, $C_2 + C_5$) = ν_{17}(Im)
	782 (4)	–	γ_{CH} (out of phase, $C_2 + C_5$) = ν_{16}(Im)
798	–	809 (137)	β_{NH_2} (wag)
	–	787 (21), 782 (10)	σ_{CC} (C_αCO)/γ_{CH} (C_2C_5)/β_{OCO}/β_{NH_2} (wag)
742	–	738 (17)	β_{OCO}/σ_{CC} ($C_\alpha C_\beta$)/γ_{CH} (C_5)
	734 (19)	–	β_{CCC} (C_β)/β_{OCO}/γ_{CH} (C_5)
	–	711 (12)	β_{CCC} (C_β)/γ_{OCO}
676	686 (75)	–	$\gamma_{COH}/\gamma_{CN/CC}$ = ν_{18}(Im)
	669 (54)	670 (63)	γ_{NH} (N_τ)
	–	639 (2)	$\gamma_{CN/CC}$
	634 (39)	–	$\gamma_{COH}/\gamma_{CN/CC}$ = ν_{20}(Im)
609	606 (26)	–	γ_{COH}/σ_{CC} (C_4C_β)
	–	606 (52)	γ_{CNC} (N_τ)
	605 (51)	–	$\gamma_{COH}/\gamma_{CN/CC}$ = ν_{19}(Im)
	–	578 (2)	β_{OCC}/β_{CCN} (N_α)
	573 (31)	–	γ_{COH}/β_{OCO}

[a] Peak positions taken from the IRMPD spectrum in Fig. 3.
[b] Vibrational frequencies (cm^{-1}) scaled by 0.975 and IR intensities (km/mol) are given in parentheses.
[c] The notation σ, β, and γ refers to stretch, in-plane bend, and out-of-plane bend modes, respectively. ν_i(Im) denote corresponding normal modes of imidazole taken from Ref. [22].

similar spectra, as do the four analogous structures for [N_α,N_π]. In contrast, the cis orientation of ∠HOCC in the higher-energy cxgc conformers of both [N_π,N_α] and [N_α,N_π] removes the OH···OC interaction such that the intense bands associated with the C—OH stretch and COH bend motions shift from ∼1140 to ∼1240 cm^{-1} and those for the CO stretch shift from ∼1780 to ∼1800 cm^{-1}. The four [N_π,CO]-cxgg conformers show similar spectra although the intense band associated with the C—OH stretch and COH bend motions is located at ∼1380 cm^{-1} (shifted because of the OH···N_α interaction) for ctg$_+$g$_-$ and ctg$_-$g$_+$ and at ∼1290 cm^{-1} for ctg$_-$g$_+$(t) and cggg, which no longer have the OH···N_α interaction. In these four cases, the CO stretch is red-shifted to ∼1745 cm^{-1}. In the four [N_π,CO]-ttgg conformers, which are all similar, the CO stretch is red-shifted even further, to 1705–1730 cm^{-1}, and

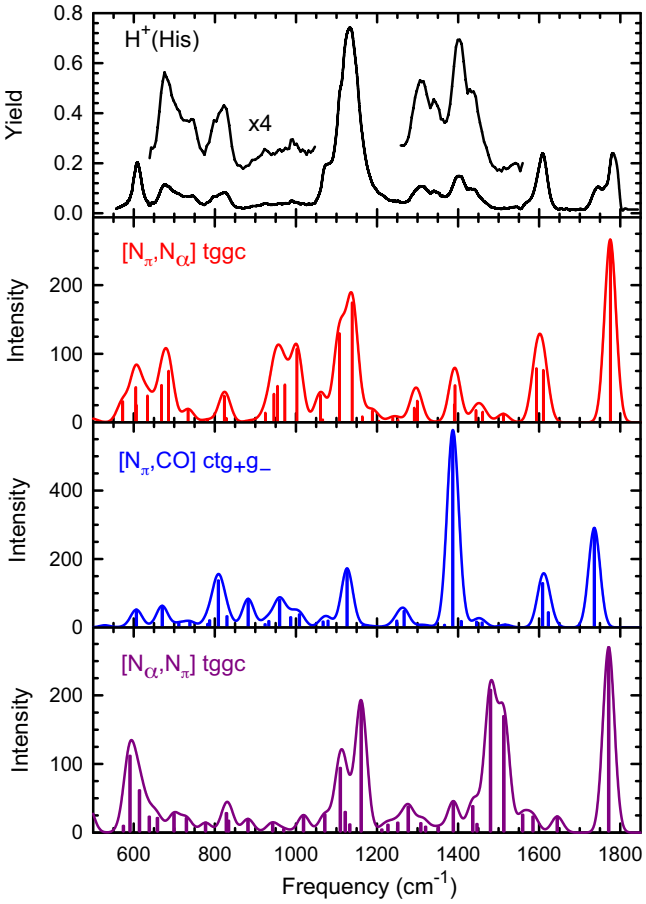

Fig. 3. Comparison of the experimental IRMPD action spectrum for H^+(His) with IR spectra for three low-lying conformations predicted at the B3LYP/6–311+G(d,p) level of theory.

the C—OH stretch and COH bend returns to ~1160 cm^{-1}. The four [N_π,OH]-txgg conformers are similar to the [N_π,CO]-ttgg analogs except the CO stretch has shifted up to ~1800 cm^{-1}.

The comparison in Fig. 3 shows that the experimental spectrum is generally consistent with that predicted for the lowest-energy conformer, [N_π,N_α]-tggc, Table 1. The principal disagreements are the lack of predicted bands at 1747 and 1340 cm^{-1}. Relative intensities are not reproduced particularly well, with predicted bands between 900 and 1000 cm^{-1} being too strong and that for the band at 1132 cm^{-1} being too weak. If the predicted bands at 1107 and 1139 cm^{-1} were closer together, as they are for the [N_π,N_α]-tgtc and ttgc conformers, Fig. S3, the agreement would improve. The carbonyl stretch in the observed spectrum at 1778 cm^{-1} is reproduced well by the [N_π,N_α]-tggc spectrum (1775 cm^{-1}), although the predicted intensity is too large. The weak bands observed are generally more delocalized bends and stretches, Table 2, but they are reproduced quite well by the [N_π,N_α] calculated spectra. The peak at 1747 cm^{-1} cannot be explained by any of the [N_π,N_α] or [N_α,N_π] conformers but is consistent with the predicted [N_π,CO]-cxgg spectra. For example, the low-lying [N_π,CO]-ctg+g− structure exhibits a red-shifted carbonyl stretch at 1736 cm^{-1}. The shift occurs because this structure forms a hydrogen bond between the protonated imidazole side-chain nitrogen (N_π) and the backbone carbonyl, whereas a weaker $N_\alpha H\cdots OC$ hydrogen bond is present in the [N_π,N_α] and [N_α,N_π] conformers, Fig. 1. The remainder of the bands predicted for [N_π,CO]-ctg+g− fall at similar positions to those of [N_π,N_α]-tggc, such that its presence is consistent with the experimental spectrum. One exception is a band at 882 cm^{-1}, where some intensity in the experimental spectrum can also be observed. We also note that the extremely intense band at 1387 cm^{-1} in the [N_π,CO]-ctg+g− spectrum, which corresponds to a COH bend and C—OH stretching motion, shifts to 1342 cm^{-1} when an anharmonic frequency calculation is performed, potentially explaining the unassigned band observed at 1340 cm^{-1}. The results of the anharmonic frequency calculation are shown for all the bands in this frequency range in Fig. S4, along with a comparable calculation for the [N_π,N_α]-tggc conformer. Few bands shift appreciably between the scaled harmonic and unscaled anharmonic calculation, so the comparison shown in Fig. 3 remains reasonable.

Although much of the spectrum shown for the [N_α,N_π]-tggc conformer can agree with the experimental spectrum, Fig. 3, there is little if any intensity observed near 1500 cm^{-1}, where the predicted spectra for all six [N_α,N_π] conformers have intense bands associated with the umbrella motion of the $N_\alpha H_3$ group. Likewise, there is no evidence in the experimental spectrum for a carbonyl stretch near 1800 cm^{-1}, suggesting that the [N_π,N_α]-cgxc, [N_α,N_π]-cgxc, and [N_π,OH] conformers are not present experimentally. Both conclusions are generally consistent with the relative energetics of these species, Table 1.

On the basis of calculated spectra and thermodynamic data, [N_π,N_α]-txxc conformers are identified as the major carrier of the measured IRMPD spectrum with total predicted populations of 68–75% and the tggc and tgtc conformers accounting for most of this intensity. [N_π,CO] conformers are predicted to account for 3–20%, consistent with the observation of the peak at 1747 cm^{-1} and perhaps that at 1340 cm^{-1}. MP2 theory suggests that the [N_α,N_π] conformers have a population of 29%, whereas the DFT calculations put this below 3%. The latter prediction seems more in line with the experimental observations, although the complex coupling between the potential wells associated with these conformations seen in Fig. 2 may complicate this conclusion.

3.4. Comparison of experimental and theoretical IR spectra: H^+(4-phenyl imidazole)

Fig. 4 shows the experimental IRMPD action spectra of H^+(PhIm) and H^+(His) compared with calculated IR spectra for the lowest energy conformer of H^+(PhIm). This structure has the proton on the imidazole nitrogen with the two rings twisted out of planarity by 35°, Fig. 4. Clearly, protonation anywhere else will be much higher in energy and the rigidity of the phenyl side-chain restricts the number of possible structures. The predicted spectrum for H^+(PhIm) shows a close correspondence to the observed spectrum, in terms of both band positions and relative intensities. The primary exception is the band at 1340 cm^{-1}, which is not predicted accurately, either because the band predicted at 1281 cm^{-1} is shifted or the band at 1326 cm^{-1} should be more intense. (An anharmonic frequency calculation for H^+(PhIm) is very similar to the scaled harmonic spectrum in Fig. 4, with no large shifts in any band having noticeable intensity.) Notably, the band at 1340 cm^{-1} in the H^+(His) spectrum was also not accurately reproduced, a comparison that might suggest that this corresponds to a motion of the imidazole side chain (in contrast to the assignment based on the anharmonic frequency calculation). Given these provisos, the experimental IRMPD action spectrum can be explained adequately by the calculated spectrum of the ground state conformer.

Detailed analysis of band positions and vibrational assignments for H^+(PhIm) are given in Table 3 on the basis of visualizing the molecular motions. Although the majority of the bands in the IRMPD spectrum of H^+(PhIm) correspond to motions throughout the molecule, the most intense bands generally involve vibrations of the imidazole ring. Only the band at 752 cm^{-1} is primarily centered in the phenyl ring, an out-of-plane CH bend. Given the non-polar nature of the phenyl ring, this seems reasonable.

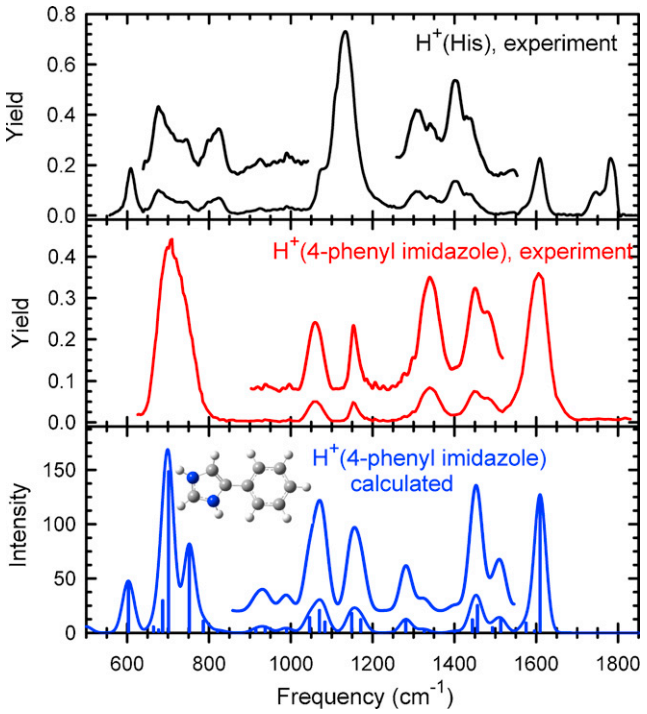

Fig. 4. Comparison of the experimental IRMPD action spectra for H^+(His) and H^+(PhIm) with the IR spectrum for protonated 4-phenyl imidazole predicted at the B3LYP/6–311+G(d,p) level of theory. The last panel also shows the calculated structure.

Comparison of the H^+(PhIm) spectrum with that of H^+(His) shows many similar features, Fig. 4. Obvious differences are that H^+(PhIm) no longer exhibits the carbonyl stretches at 1750–1800 cm^{-1} nor the band at 1139 cm^{-1} corresponding to the COH bend and C—OH stretch, which gives much of the intensity to the 1132 cm^{-1} peak in the H^+(His) spectrum. Likewise, the band at about 700 cm^{-1} in H^+(PhIm) is enhanced by contributions from the phenyl group. One interesting difference in the two spectra is the apparent shift in the bands at 1399 and 1433 cm^{-1} for H^+(His) to 1448 and 1482 cm^{-1} for H^+(PhIm). Actually, the predicted band positions between the two molecules do not change appreciably in this region, but intensities vary because some modes gain in intensity by interactions with the polar amino acid group in His. For example, the band at 1399 cm^{-1} for H^+(His), which corresponds mainly to an in-plane $N_\pi H$ bend, is not observed for H^+(PhIm) because its predicted intensity has dropped by a factor of 33. Overall, this comparison demonstrates the contributions that the imidazole side-chain make to the spectrum of H^+(His).

3.5. Comparison of experimental IR spectra: H^+(His) versus H^+(histamine)

In a recent study, Lagutschenkov et al. [22] published a detailed analysis of the IRMPD spectrum of protonated histamine, a neurotransmitter, which is His without the carboxylic acid on the **α**-carbon. They compared the experimental IRMPD spectrum of protonated histamine with predicted IR spectra of several low-energy structures, which were characterized by quantum-chemical calculations at the B3LYP and MP2 levels of theory using the cc-pVDZ basis set. These calculations predict the most stable conformer is the imidazolium-type conformer with protonation at the imidazole ring and gauche conformation of the ethylamine side chain, which is significantly stabilized by an intramolecular ionic $N_\pi H\cdots N_\alpha$ hydrogen bond. This structure is equivalent to the $[N_\pi,N_\alpha]$ conformers for H^+(His), Fig. 1, which are all the same once H replaces the COOH group. Close in energy is the gauche ammonium-type N_α tautomer, equivalent to $[N_\alpha,N_\pi]$ conformers of H^+(His). All other conformations found for H^+(histamine) no longer contain the $N_\pi\cdots H\cdots N_\alpha$ hydrogen bond and are therefore much higher in energy (>32 kJ/mol). Similar to the findings discussed above for the analogous H^+(His) complexes, B3LYP calculations prefer H^+(histamine) $[N_\pi,N_\alpha]$, the imidazolium ion structure, by 6.3 kJ/mol, whereas MP2 calculations stabilize the $[N_\alpha,N_\pi]$, the ammonium ion structure, actually finding that it lies lower in energy by 1.7 kJ/mol. Larger basis sets shift the balance back to the $[N_\pi,N_\alpha]$ structure, with the relative differences between B3LYP and MP2 remaining. These results are confirmed here where, for the three levels of theory used above, the $[N_\pi,N_\alpha]$-type is the ground state by 7.8 (B3LYP), 5.2 (B3P86), and −0.1 (MP2) kJ/mol, respectively.

Good agreement was found between and the experimental spectrum and the predicted spectrum for H^+(histamine) $[N_\pi,N_\alpha]$, whereas the $[N_\alpha,N_\pi]$ structure was concluded to contribute only a minor amount to the observed spectrum. Interestingly, as Lagutschenkov et al. point out, all other related protonated neurotransmitter ions studied to date prefer protonation at the

Table 3
Experimental vibrational frequencies (cm^{-1}) of H^+(4-phenyl imidazole) compared to B3LYP/6–311+G(d,p) frequencies.

H^+(PhIm) ν_{exp} [a]	H^+(PhIm), ν_{cal} [b]	Vibration[c]
1606	1609 (126)	$\sigma_{CC}(C_4C_5)/\beta_{NH}$ (N_π,N_τ)/β_{CH} (C_5) = ν_5(Im)
	1596 (2)	σ_{CC}(Ph,sym)/β_{CH} (Ph)
	1575 (9)	σ_{CC}(Ph,antisym)/β_{CH} (Ph)
1482	1513 (12)	$\sigma_{CN}(C_2)/\beta_{CH}$ (C_2,C_5) = ν_6(Im)
	1493 (5)	β_{CH}(Ph)/σ_{CC} (C_4C_{Ph})/β_{NH} (N_τ)
1448	1456 (25)	$\beta_{NH}(N_\tau)/\sigma_{CN}$ (N_τ)
	1444 (12)	β_{CH}(Ph)/σ_{CC}(Ph,antsym)
	1401 (2)	$\beta_{NH}(N_\pi)/\sigma_{CN}$ (N_π) = ν_7(Im)
1339	1326 (3)	β_{CH}(Ph,antisym)
	1302 (1)	σ_{CC}(Ph,antisym)/β_{CH} (Ph)
~1300 (tail)	1281 (12)	$\sigma_{CN}(C_5N_\tau)/\beta_{CH}$ (C_5)/β_{CH_2} (wag) = ν_{10}(Im)
	1234 (0.2)	$\sigma_{CN}(C_4N_\pi)/\beta_{CH}$ (C_5)/β_{NH} (N_π) = ν_8(Im)
	1181 (1)	β_{CH}(Ph,sym)
1152	1171 (12)	$\beta_{CH}(C_2)/\beta_{NH}$ (N_τ) = ν_9(Im)
	1164 (0.1)	β_{CH}(Ph)
	1149 (18)	$\beta_{CH}(C_2)/\beta_{NH}(N_\pi)$ = ν_{12}(Im)
	1084 (10)	β_{CH}(Ph)/σ_{CC} (Ph)
1064	1070 (21)	$\sigma_{CN}(C_5N_\tau)/\beta_{CH}$ (C_5) = ν_{11}(Im)
	1046 (14)	$\sigma_{CN}(C_4N_\pi)/\beta_{CH}$ (C_5)/β_{CH} (Ph)
996	990 (4)	σ_{CC}(Ph,sym)
	970 (1)	γ_{CH}(Ph)
937	937 (5)	$\sigma_{CN}(N_\pi$,sym) = ν_{14}(Im)
	918 (1)	γ_{CH}(Ph)
	915 (3)	β (NC_2N) = ν_{15}(Im)
	830 (1)	γ_{CH}(Ph,out of phase)
	821 (1)	γ_{CH} (in phase, C_2+C_5) = ν_{17}(Im)
	786 (11)	γ_{CH} (out of phase, C_2+C_5) = ν_{16}(Im)
	752 (81)	γ_{CH}(Ph)
~710 (wide)	701 (149)	γ_{NH} (in phase, $N_\pi+N_\tau$)
	687 (30)	γ_{CH}(Ph)
	677 (3)	β_{CC}(Ph)
	664 (6)	$\gamma_{CN/CC}$ = ν_{18}(Im)
	649 (0.2)	γ_{NH} (out of phase, $N_\pi+N_\tau$)
	603 (48)	$\gamma_{CN/CC}$ = ν_{19}(Im)

[a] Peak positions taken from the IRMPD spectrum in Fig. 4.
[b] Vibrational frequencies (cm^{-1}) scaled by 0.975 and IR intensities (km/mol) are given in parentheses.
[c] The notation σ, β, γ, and τ refers to stretch, in-plane bend, out-of-plane bend, and torsional modes, respectively. Im and Ph refer to imidazole and phenyl, respectively. ν_i(Im) denote corresponding normal modes of imidazole taken from Ref. [22].

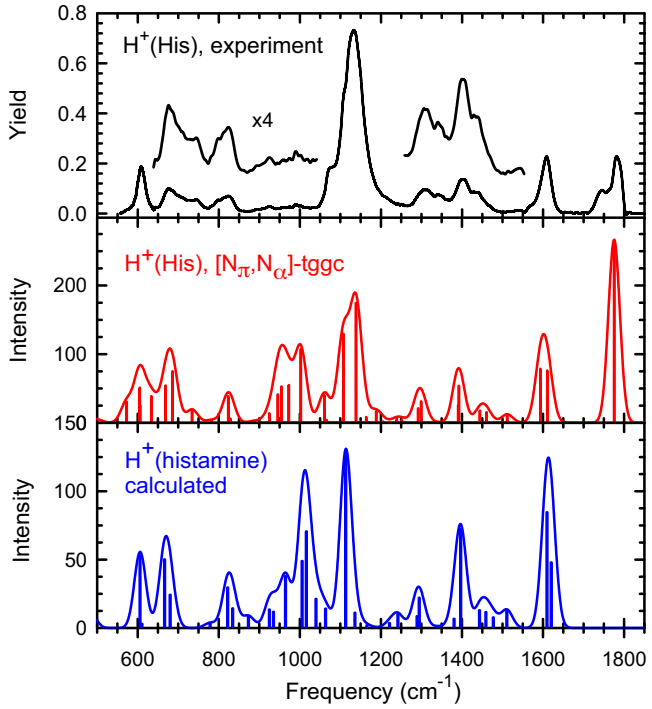

Fig. 5. Comparison of the experimental IRMPD action spectra for H^+(His) with IR spectra for H^+(His)[N_π,N_α]-tggc and H^+(histamine) predicted at the B3LYP/6–311+G(d,p) level of theory.

alkylamino side chain, such that histamine is unique in its preference for imidazole protonation.

The IRMPD action spectra of H^+(His) and H^+(histamine) have many similar features. Bands at 1609, 1433, 1399, 1340, 1306, 1132, 1079, ~990, ~923, 822, 798, 676, and 609 cm^{-1} in the spectrum of H^+(His) are observed at 1598, 1453, 1389, 1359, 1293, 1107, 1075, 997, 909, 830, 788, 685, and 607 cm^{-1} in the protonated histamine spectrum. This can be seen by a comparison of the B3LYP/6–311+G(d,p) calculated spectra in Fig. 5. Carbonyl stretches (1778 and 1747 cm^{-1}) and the OCO bend (742 cm^{-1}) in the H^+(His) spectrum are not observed for protonated histamine for obvious reasons. Likewise, the COH bend and C—OH stretch contributes to the experimental band in H^+(His) at 1132 cm^{-1}, thereby blue shifting it from the 1107 cm^{-1} observed for H^+(histamine), assigned to mainly an in-plane N_πH bend. Overall, this comparison is consistent with the assignment above, namely, that the [N_π,N_α] form of H^+(His) dominates the experimental spectrum, with additional contributions from the [N_π,CO] form, which is not available to H^+(histamine).

In making this comparison, we did note one interesting anomaly in comparing IR spectra for the most stable conformer of H^+(histamine) calculated at the B3LYP/6–311+G(d,p) level compared with that reported by Lagutschenkov et al. [22]. They agree well over the experimental range examined in most respects, with average deviations between band positions of 6 ± 6 cm^{-1} except for the band associated with the out-of-plane N_πH bend, i.e., a proton motion perpendicular to the N_π–$H^+\cdots N_\alpha$ hydrogen bond. Here, our predicted frequency (1016 cm^{-1}, 0.975 scaling) differs by 62 cm^{-1} (after scaling,) with that for the B3LYP/cc-pVDZ calculations (1078 cm^{-1}, 0.98 scaling), where the latter agree better with experiment (1075 cm^{-1}). This difference appears to be exclusively one related to the size of the basis set as B3LYP/aug-cc-pVDZ, B3LYP/cc-pVTZ, and B3LYP/aug-cc-pVTZ calculations yield frequencies for this motion of 1036, 1026, and 1018 cm^{-1} (0.98 scaling); however, this frequency is nearly unique in this regard. For example, the in-plane bend of the same N_πH has calculated frequencies of 1117, 1114, 1121, 1118 (0.98 scaling), and 1113 cm^{-1} (0.975 scaling) for cc-pVDZ, aug-cc-pVDZ, cc-pVTZ, aug-cc-pVTZ, and 6–311+G(d,p) basis sets. All other frequencies in the experimental range of interest agree with one another with similarly small variations.

3.6. Comparison of experimental IR spectra: H^+(His) and $His^{\bullet+}$

Recently, Steill et al. [23] used IRMPD spectroscopy to study the histidine radical cation. They compared the experimental IRMPD spectrum of $His^{\bullet+}$ with predicted IR spectra of several low energy structures, finding a good match with the predicted IR spectrum of the global minimum structure, a captodative radical ion that has a structure essentially the same as [N_π,CO]-ttg$_+$g$_-$(t) shown in Fig. 1 but without the hydrogen atom on the α-carbon. Notably this radical center allows the H_2N–C–COOH atoms to be nearly coplanar, allowing resonant stabilization along the NCCO atoms and a shorter $N_\pi H\cdots$OC hydrogen bond, 1.68 Å compared to 1.78 Å for [N_π,CO]-ttg$_+$g$_-$(t) as calculated at the B3LYP/6–311+G(d,p) level. The IRMPD action spectra of H^+(His) and $His^{\bullet+}$ have many similar features. Bands comparable to those at 1609, 1399, 1132, 822, 742, 676, and 609 cm^{-1} in the spectrum of H^+(His) are also observed in the $His^{\bullet+}$ spectrum. Key differences in the spectra are shifts in the observed carbonyl stretches for H^+(His) at 1778 and 1747 cm^{-1} to 1666 cm^{-1} for $His^{\bullet+}$, and the presence of a band at about 1490 cm^{-1} for $His^{\bullet+}$, which corresponds to stretches along the $N_\alpha C_\alpha$CO backbone. The latter band clearly shifts because of the resonant delocalization associated with the radical center. Comparison of the [N_π,N_α] and [N_π,CO] spectra of Fig. 3 also shows a red shift in the carbonyl stretch resulting from the stronger $N_\pi H\cdots$OC hydrogen bond in the latter structure (and $His^{\bullet+}$), but not as large a shift as for $His^{\bullet+}$. This demonstrates that the resonant delocalization from the C_α radical center of $His^{\bullet+}$ removes electron density from the carbonyl π bond, weakening it further.

It is also interesting to consider why an [N_π,N_α] binding motif is no longer energetically favorable for $His^{\bullet+}$, as found for H^+(His). Although an exhaustive search for conformations was not conducted, calculations for $His^{\bullet+}$ at the present levels of theory find the captodative radical analog of [N_π,N_α]-tggc to lie 42–43 kJ/mol higher in energy than the [N_π,CO] ground state. These calculations show that the NH_2 amino group in the [N_π,N_α] conformer is no longer nearly planar, becoming pyramidal in order to form the $N_\pi H\cdots N_\alpha$ hydrogen bond, thereby losing the resonant stabilization of the radical noted above.

3.7. Comparison of experimental IR spectra: H^+(His) versus H^+(HisArg) and H_2^{2+}(HisArg)

The Williams group has examined H^+(HisArg) and H_2^{2+}(HisArg) with IRMPD spectroscopy and theory [53]. The IRMPD action spectra of H^+(His) and H^+(HisArg), the latter protonated on the Arg side chain, have some similar features. The observed carbonyl stretch (1788 cm^{-1}), NH bends (~1650 cm^{-1}), and in-plane hydroxyl bend (1150 cm^{-1}) in the H^+(HisArg) spectrum are also seen for H^+(His) at 1778, 1609, 1132 cm^{-1}, respectively. A sharp, intense peak at 1080 cm^{-1} is observed for H^+(HisArg) that is attributed to the neutral histidine side chain on the basis of a comparison to the IR spectra of condensed phase imidazole. Consistent with this assignment is the observation that protonation of the imidazole side chain in the IRMPD spectrum of H_2^{2+}(HisArg) decreases the intensity of this peak appreciably, becoming a shoulder on the intense 1150 cm^{-1} band. This is comparable to the shoulder observed at 1079 cm^{-1} in the H^+(His) spectrum, Fig. 3, consistent with protonation of the imidazole ring.

3.8. Comparison of experimental IR spectra: H^+(His) versus M^+(His)

We can also compare the experimental IRMPD spectrum for H^+(His) with that for alkali metal cation complexes, M^+(His), where $M^+ = Li^+$, Na^+, K^+, Rb^+, and Cs^+ [25]. There are several similarities although most bands are broader in the protonated species. The highest frequency band corresponding to the carbonyl stretch at 1778 cm^{-1} for H^+(His) is compared to 1732–1753 cm^{-1} for the alkali metal complexes. Clearly, the hydrogen bond between the protonated imidazole side-chain nitrogen and backbone amino nitrogen perturbs the carbonyl stretch less than direct binding to the heavier alkali cations. An intense band at 1125–1157 cm^{-1} is observed in all spectra, consistent with the fact that the COH bending and C—OH stretching motions of the H^+(His) [N_π,N_α] and M^+(His) [CO,N_α,N_π] conformers are similar. The latter complex is a tridentate structure in which the metal cation binds to the carbonyl and amino group of the backbone along with the N_π nitrogen of the side-chain. The shoulder at 1079 cm^{-1} in the H^+(His) spectrum becomes a sharp, isolated band in the spectra of all M^+(His) complexes. This is consistent with its identification as a signature peak associated with a neutral imidazole side chain at 1080 cm^{-1} [53,54] and attributed to CN stretches and in-plane CH and NH bends of the side chain ring. Observed bands at ~1580 cm^{-1} in the K^+(His)–Cs^+(His) spectra correspond to an NH_2 bend in the [CO,N_α,N_π] spectra. The comparable band in the H^+(His) spectrum is found at 1609 cm^{-1}, again consistent with more perturbation induced by direct metal binding to the N_α site.

The theoretical results for K^+(His)–Cs^+(His) indicate that the bidentate [CO,N_π] conformer, in which the metal cation binds to the backbone carbonyl oxygen and nitrogen atom of the imidazole side chain, has an intense band near 1400 cm^{-1}, corresponding to the COH bending motion. This motion is largely unaffected by the increasing cation size, being observed at ~1390, ~1385, and ~1394 cm^{-1} for K^+(His)–Cs^+(His). This is also true for H^+(His) [N_π,CO], being predicted at 1387 cm^{-1} and observed at 1399 cm^{-1}. Similarly, weak bands at 742, 822, and 1433 cm^{-1} are observed in all cationized spectra, from Li^+(His) to Cs^+(His), which seems reasonable as these frequencies correspond to motions that mainly involve groups not directly attached to the ion. Interestingly, the former two frequencies become more prominent as the cation size increases, which is consistent with the increasing populations of [CO,N_π] and [COOH] conformations for which these modes gain intensity compared to [CO,N_α,N_π]. The weak band observed at ~990 cm^{-1} in H^+(His), largely the NH_2 wag, can be found in all the M^+(His) spectra but has appreciable intensity only in the Li^+(His) spectrum, suggesting that the higher charge density may enhance the intensity of this mode. The band observed at 676 cm^{-1} in H^+(His) is absent in all the M^+(His) spectra, consistent with the predicted IR intensities for these motions, which are greatly reduced for the metal systems.

4. Conclusions

The gas-phase structures of protonated histidine (His) and the side-chain model, protonated 4-phenyl imidazole (PhIm), are examined by infrared multiple photon dissociation (IRMPD) action spectroscopy utilizing light generated by the free electron laser FELIX. Comparison of the measured IRMPD spectra to single photon absorption results calculated at a B3LYP/6–311+G(d,p) level of theory show that H^+(His) is characterized by a [N_π,N_α] conformer along with some [N_π,CO]. These conformers have the protonated nitrogen atom of imidazole adjacent to the side-chain (N_π) hydrogen bonding to the backbone amino nitrogen (N_α) and to the backbone carbonyl oxygen, respectively. Comparison of the spectra for H^+(PhIm) and H^+(His) allows identification of the vibrational contributions from the protonated imidazole side-chain. Likewise, the IRMPD action spectra of H^+(His) and H^+(histamine) [22], which is His without the carboxylic acid on the α-carbon, are found to share many similar features. Comparison of the IRMPD spectra of H^+(His) with that of the $His^{\bullet+}$ radical cation provides further evidence for the resonant electron delocalization from the C_α radical center of $His^{\bullet+}$ that is characteristic of the captodative radical ion identified by Steill et al. [23]. When compared to results for H^+(HisArg), $H_2{}^{2+}$(HisArg) [53], and M^+(His) [25], the IRMPD action spectrum of H^+(His) is consistent with protonation of the imidazole ring in only H^+(His) and $H_2{}^{2+}$(HisArg). Trends in the frequencies observed for M^+(His), where $M^+ = H^+$, Li^+, Na^+, K^+, Rb^+, and Cs^+, are also explained.

Acknowledgments

Financial support was provided by the National Science Foundation, Grants PIRE-0730072 and CHE-1049580. This work is also part of the research program of FOM, which is financially supported by the Nederlandse Organisatie voor Wetenschappelijk Onderzoek (NWO). The skillful assistance of the FELIX staff, in particular Lex van der Meer, Britta Redlich, Giel Berden, and Josipa Grzetic, is gratefully acknowledged. In addition, we thank the Center for High Performance Computing at the University of Utah for the generous allocation of computer time.

Appendix A. Supplementary data

Supplementary data associated with this article can be found, in the online version, at http://dx.doi.org/10.1016/j.ijms.2012.06.002.

References

[1] A. Roth, R.R. Breaker, Proceedings of the National Academy of Sciences of the United States of America 95 (1998) 6027.
[2] A.-M.A. Hays, I.R. Vassiliev, J.H. Golbeck, R.J. Debus, Biochemistry 37 (1998) 11352.
[3] A. Warshel, S. Russell, Journal of the American Chemical Society 108 (1986) 6569.
[4] C. Tu, D.N. Silverman, C. Forsman, B.H. Jonsson, S. Lindskog, Biochemistry 28 (1989) 7913.
[5] P.A. Frey, S.A. Whitt, J.B. Tobin, Science 264 (1994) 1927.
[6] M.A. Walters, T.G. Spiro, Inorganic Chemistry 22 (1983) 4014.
[7] D.S. Caswell, T.G. Spiro, Journal of the American Chemical Society 108 (1986) 6470.
[8] J. Ramsden, T.G. Spiro, Biochemistry 28 (1989) 3125.
[9] E.A. Dierks, S. Hu, K.M. Vogel, A.E. Yu, T.G. Spiro, J.N. Burstyn, Journal of the American Chemical Society 119 (1997) 7316.
[10] X. Zhao, D. Wang, T.G. Spiro, Inorganic Chemistry 37 (1998) 5414.
[11] X. Zhao, D. Wang, T.G. Spiro, Journal of the American Chemical Society 120 (1998) 8517.
[12] M. Vargek, X. Zhao, Z. Lai, G.L. McLendon, T.G. Spiro, Inorganic Chemistry 38 (1999) 1372.
[13] D. Wang, X. Zhao, M. Vargek, T.G. Spiro, Journal of the American Chemical Society 122 (2000) 2193.
[14] Q. Wu, G. Balakrishnan, A. Pevsner, T.G. Spiro, Journal of Physical Chemistry A 107 (2003) 8047.
[15] S. Hashimoto, S. Ohsaka, H. Takeuchi, I. Harada, Journal of the American Chemical Society 111 (1989) 8926.
[16] S. Hashimoto, H. Takeuchi, Journal of the American Chemical Society 120 (1998) 11012.
[17] S. Hashimoto, H. Takeuchi, Biochemistry 45 (2006) 9660.
[18] A. Okada, T. Miura, H. Takeuchi, Biochemistry 40 (2001) 6053.
[19] T. Noguchi, Y. Inoue, X.-S. Tang, Biochemistry 38 (1998) 399.
[20] Z. Huang, Z. Lin, C. Song, Journal of Physical Chemistry A 111 (2007) 4340.
[21] K. Hasegawa, T.-A. Ono, T. Noguchi, Journal of Physical Chemistry B 104 (2000) 4253.
[22] A. Lagutschenkov, J. Langer, G. Berden, J. Oomens, O. Dopfer, Physical Chemistry Chemical Physics 13 (2011) 15644.
[23] J. Steill, J. Zhao, C.-K. Siu, Y. Ke, U.H. Verkerk, J. Oomens, R.C. Dunbar, A.C. Hopkinson, K.W.M. Siu, Angewandte Chemie International Edition 47 (2008) 9666.
[24] J.T. O'Brien, J.S. Prell, G. Berden, J. Oomens, E.R. Williams, International Journal of Mass Spectrometry 297 (2010) 116.
[25] M. Citir, C.S. Hinton, J. Oomens, J.D. Steill, P.B. Armentrout, Journal of Physical Chemistry A 116 (2012) 1532.

[26] D. Oepts, A.F.G. van der Meer, P.W. van Amersfoort, Infrared Physics and Technology 36 (1995) 297.
[27] J.J. Valle, J.R. Eyler, J. Oomens, D.T. Moore, A.F.G.v.d. Meer, G.v. Heldon, G. Meijer, C.L. Hendrickson, A.G. Marschall, G.T. Blakney, Review of Scientific Instruments 76 (2005) 023103.
[28] N.C. Polfer, J. Oomens, D.T. Moore, G. von Helden, G. Meijer, R.C. Dunbar, Journal of the American Chemical Society 128 (2006) 517.
[29] N.C. Polfer, J. Oomens, Physical Chemistry Chemical Physics 9 (2007) 3804.
[30] R.M. Moision, P.B. Armentrout, Journal of Physical Chemistry A 106 (2002) 10350.
[31] D.A. Pearlman, D.A. Case, J.W. Caldwell, W.R. Ross, T.E. Cheatham, S. DeBolt, D. Ferguson, G. Seibel, P. Kollman, Computer Physics Communications 91 (1995) 1.
[32] E.J. Bylaska, W.A. deJong, K. Kowalski, T.P. Straatsma, M. Valiev, D. Wang, E. Aprà, T.L. Windus, S. Hirata, M.T. Hackler, Y. Zhao, P.-D. Fan, R.J. Harrison, M. Dupuis, D.M.A. Smith, J. Nieplocha, V. Tipparaju, M. Krishnan, A.A. Auer, M. Nooijen, E. Brown, G. Cisneros, G.I. Fann, H. Früchtl, J. Garza, K. Hirao, R. Kendall, J.A. Nichols, K. Tsemekhman, K. Wolinski, J. Anchell, D. Bernholdt, P. Borowski, T. Clark, D. Clerc, H. Dachsel, M. Deegan, K. Dyall, D. Elwood, E. Glendening, M. Gutowski, A. Hess, J. Jaffe, B. Johnson, J. Ju, R. Kobayashi, R. Kutteh, Z. Lin, R. Littlefield, X. Long, B. Meng, T. Nakajima, S. Niu, L. Pollack, M. Rosing, G. Sandrone, M. Stave, H. Taylor, G. Thomas, J.v. Lenthe, A. Wong, Z. Zhang, NWChem, A Computational Chemistry Package for Parallel Computers, Pacific Northwest National Laboratory, Richland, Washington 99352, 2003.
[33] C.C. Roothaan, Reviews of Modern Physics 23 (1951) 69.
[34] J.S. Binkley, J.A. Pople, W.J. Hehre, Journal of the American Chemical Society 102 (1980) 939.
[35] M.J. Frisch, G.W. Trucks, H.B. Schlegel, G.E. Scuseria, M.A. Robb, J.R. Cheeseman, G. Scalmani, V. Barone, B. Mennucci, G.A. Petersson, H. Nakatsuji, M. Caricato, X. Li, H.P. Hratchian, A.F. Izmaylov, J. Bloino, G. Zheng, J.L. Sonnenberg, M. Hada, M. Ehara, K. Toyota, R. Fukuda, J. Hasegawa, M. Ishida, T. Nakajima, Y. Honda, O. Kitao, H. Nakai, T. Vreven, J. Montgomery, J.A.J.E. Peralta, F. Ogliaro, M. Bearpark, J.J. Heyd, E. Brothers, K.N. Kudin, V.N. Staroverov, R. Kobayashi, J. Normand, K. Raghavachari, A. Rendell, J.C. Burant, J.M. Millam, S.S. Iyengar, J. Tomasi, M. Cossi, N. Rega, J.M. Millam, M. Klene, J.E. Knox, J.B. Cross, V. Bakken, C. Adamo, J. Jaramillo, R. Gomperts, R.E. Stratmann, O. Yazyev, A.J. Austin, R. Cammi, C. Pomelli, J.W. Ochterski, R.L. Martin, K. Morokuma, V.G. Zakrzewski, G.A. Voth, P. Salvador, J.J. Dannenberg, S. Dapprich, A.D. Daniels, O. Farkas, J.B. Foresman, J.V. Ortiz, J. Cioslowski, D.J. Fox, Gaussian 09, Revision A.02, Gaussian Inc., Pittsburgh, PA, 2009.
[36] A.D. Becke, Journal of Chemical Physics 98 (1993) 5648.
[37] R. Ditchfield, W.J. Hehre, J.A. Pople, Journal of Chemical Physics 54 (1971) 724.
[38] A.D. McLean, G.S. Chandler, Journal of Chemical Physics 72 (1980) 5639.
[39] J.B. Foresman, A.E. Frisch, Exploring Chemistry with Electronic Structure Methods, Gaussian, Inc., Pittsburgh, PA, 1996.
[40] N.C. Polfer, J. Oomens, R.C. Dunbar, Physical Chemistry Chemical Physics 8 (2006) 2744.
[41] M.F. Bush, J. Oomens, R.J. Saykally, E.R. Williams, Journal of Physical Chemistry A 112 (2008) 8578.
[42] M.F. Bush, J. Oomens, R.J. Saykally, E.R. Williams, Journal of the American Chemical Society 130 (2008) 6463.
[43] A.L. Heaton, V.N. Bowman, J. Oomens, J.D. Steill, P.B. Armentrout, Journal of Physical Chemistry A 113 (2009) 5519.
[44] D.R. Carl, T.E. Cooper, J. Oomens, J.D. Steill, P.B. Armentrout, Physical Chemistry Chemical Physics 12 (2010) 3384.
[45] M. Citir, E.M.S. Stennett, J. Oomens, J.D. Steill, M.T. Rodgers, P.B. Armentrout, International Journal of Mass Spectrometry 297 (2010) 9.
[46] S.J. Ye, P.B. Armentrout, Journal of Physical Chemistry A 112 (2008) 3587.
[47] T.E. Cooper, D.R. Carl, P.B. Armentrout, Journal of Physical Chemistry A 113 (2009) 13727.
[48] P.B. Armentrout, A.L. Heaton, S.J. Ye, Journal of Physical Chemistry A 115 (2011) 11144.
[49] D.R. Carl, P.B. Armentrout, Journal of Physical Chemistry A 116 (2012) 3802.
[50] H.E. Aribi, G. Orlova, A.C. Hopkinson, K.W.M. Siu, Journal of Physical Chemistry A 108 (2004) 3844.
[51] F. Rogalewicz, Y. Hoppilliard, G. Ohanessian, International Journal of Mass Spectrometry 195/196 (2000) 565.
[52] IUPAC, Compendium of Chemical Terminology (the Gold Book), 2nd ed., Compiled by A.D. McNaught, A. Wilkinson, Blackwell Scientific Publications, Oxford, 1997 (XML on-line corrected version: http://goldbook.iupac.org (2006) created by M. Nic, J. Jirat, B. Kosata, updates compiled by A. Jenkins, ISBN 0-9678550-9-8, http://dx.doi.org/10.1351/goldbook).
[53] J.S. Prell, J.T. O'Brien, J.D. Steill, J. Oomens, E.R. Williams, Journal of the American Chemical Society 131 (2009) 11442.
[54] M.C. Sister, J.L. Walter, Spectrochimica Acta, Part A 24 (1968) 237.